Cholinergic modulation of dentate gyrus processing through dynamic reconfiguration of inhibitory circuits

Mora B. Ogando[1], Noel Federman[1], Sebastián A. Romano[1], Luciano A. Brum[2], Guillermo M. Lanuza[2], Damian Refojo[1], Antonia Marin-Burgin[1*]

1. Instituto de Investigación en Biomedicina de Buenos Aires (IBioBA) –
CONICET - Partner Institute of the Max Planck Society
Godoy Cruz 2390, C1425FQD, Buenos Aires, Argentina

2. Fundación Instituto Leloir-Instituto de Investigaciones Bioquímicas de Buenos Aires-Consejo Nacional de Investigaciones Científicas y Técnicas (CONICET), Av. Patricias Argentinas 435, Buenos Aires C1405BWE, Argentina.

Short Title: Cholinergic modulation of dentate gyrus processing

*Correspondence should be addressed to aburgin@ibioba-mpsp-conicet.gov.ar

ABSTRACT

The dentate gyrus (DG) of the hippocampus plays a key role in memory formation and it is known to be modulated by septal projections. By performing electrophysiology and optogenetics we evaluated the role of cholinergic modulation in the processing of afferent inputs in the DG. We showed that mature granule cells (GCs), but not adult-born immature neurons, have increased responses to afferent perforant path stimuli upon cholinergic modulation. This is due to a highly precise reconfiguration of inhibitory circuits, differentially affecting Parvalbumin and Somatostatin interneurons, resulting in a nicotinic-dependent feedforward perisomatic disinhibition of GCs. This circuit reorganization provides a mechanism by which mature GCs could escape the strong inhibition they receive, creating a window of opportunity for plasticity. Indeed, coincident activation of perforant path inputs with optogenetic release of Ach produced a long-term potentiated response in GCs, which could be crucial for the formation of memories.

INTRODUCTION

The dentate gyrus (DG), the main entrance of information to the hippocampus from the entorhinal cortex (EC, Andersen et al., 1971), plays a key role in the formation of new memories and memory associations in mammals (Marr, 1971, Burgess et al., 2002, Leutgeb et al., 2005). It is thought to separate the rich repertoire of inputs arriving from EC into non-overlapping sparse patterns of activity, improving discriminability and reducing interference between stored representations (Leutgeb et al., 2007, Bakker et al., 2008, Neunuebel and Knierim, 2014). The sparsity in the activity of granule cells (GCs), the principal neuron type of the DG, is governed by strong local GABAergic inhibition (Nitz and McNaughton, 2004, Pernia-Andrade and Jonas, 2014). However, the mechanisms that allow GCs to surmount this basal inhibitory suppression in order to undergo the activity-dependent plastic changes related to memory are still unclear. In the hippocampus, synaptic inhibition is provided by two main interneuron types, parvalbumin-expressing perisomatic-inhibiting fast-spiking interneurons (PVIs) and somatostatin-expressing dendrite-inhibiting cells (SOMIs) (Freund and Buzsaki, 1996, Rudy et al., 2011, Hosp et al., 2014). PVIs provide powerful feedforward and feedback inhibition to large populations of GCs (Sambandan et al., 2010) and they are critical for the generation of gamma activity (Bartos et al., 2007, Struber et al., 2017). On the other hand, SOMIs (i.e. classically called hilar-perforant-path-associated interneurons-HIPPs) distribute axon fibers along the molecular layer, and are engaged by converging GC-inputs providing mostly dendritic feedback inhibition to the DG circuitry (Yuan et al., 2017).

The GC population is heterogeneous, mostly due to the existence of adult neurogenesis in the DG (van Praag et al., 2002). In vivo, the distribution of GC´s firing rates is typically bimodal with long periods of quiescence punctuated by high frequency activity bursts (Jung and McNaughton, 1993, Mistry et al., 2011). Interestingly, these bursting periods when GCs are able to escape the predominant inhibition, occur frequently upon active exploration of behaviorally relevant cues (Mistry et al., 2011, Sasaki et al., 2018). In addition, there is evidence for subpopulations of GCs with more unimodal low frequency firing rate distributions in vivo (Mistry et al., 2011). The electrophysiological and functional

differences between populations are presumably related to maturity. Immature GCs are more excitable and less selective, responding to a wider range of frequencies and are more prone to plastic changes than mature GCs (Ge et al., 2007, Mongiat et al., 2009, Marín-Burgin et al., 2012, Pardi et al., 2015). The disparity is mostly given by a difference in perisomatic feedforward inhibition of GCs, which is underdeveloped in immature GCs (Espósito et al., 2005, Marín-Burgin et al., 2012). Furthermore, place fields of immature adult born neurons are known to be broad, but become sharper and more spatially tuned with maturation (Danielson et al., 2016), suggesting that this population could process different information compared to mature cells (Marin-Burgin and Schinder, 2012, Nakashiba et al., 2012, Denny et al., 2014).

Despite their sparse activation, reduced excitability and higher threshold for LTP induction, several studies have shown that mature GCs participate in the formation of memory engrams (Stone et al., 2011, Liu et al., 2012, Ramirez et al., 2013, Ryan et al., 2015, Tronel et al., 2015). In order to be integrated into engrams, mature GCs have to overcome the strong inhibition they receive. Although some suggested cell-intrinsic properties could allow them to undergo plasticity (Lopez-Rojas et al., 2016, Lopez-Rojas and Kreutz, 2016), circuital mechanisms could also be involved. One hypothesis is that neuromodulators could adapt circuit processing to allow for plasticity (Palacios-Filardo and Mellor, 2018). The DG receives a number of neuromodulatory inputs that are able to alter the information processing properties of specific populations of neurons (Prince et al., 2016, Palacios-Filardo and Mellor, 2018). Among them, the cholinergic afferents, arriving primarily from the medial forebrain (Mesulam et al., 1983, Wainer et al., 1985), play an important role in modulating cortical circuit activity (Dannenberg et al., 2017). Several lines of evidence indicate a role for acetylcholine (ACh) in hippocampal-related cognitive functions, including coding of spatial location, movement speed, learning and memory (Haam and Yakel, 2017), attention to sensory stimuli (Sarter et al., 2005, Pinto et al., 2013, Bloem et al., 2014). ACh is thought to exert modulatory actions in cortical circuits both via direct synaptic contacts (Parikh et al., 2007, Letzkus et al., 2011) and through diffusion by volume transmission (Hasselmo and McGaughy, 2004, Sarter et al.,

2009). Microdialysis studies, which have a temporal resolution of minutes have shown an increase in tonic ACh release in the hippocampus during attention, stress, exploration, and locomotion (Pepeu and Giovannini, 2004). On the other hand, phasic ACh release was strongly associated with reward delivery in a working memory task (Teles-Grilo Ruivo et al., 2017). One striking cellular effect caused by increasing cholinergic activity in the hippocampus is the enhancement of the impact of feedforward afferent inputs´, while simultaneously suppressing the influence of excitatory feedback connections (Hasselmo, 2006).

Although much is known about the role of ACh as a modulator of information flow at CA1 and CA3 hippocampal subregions, cholinergic modulation of the DG microcircuit has been less explored. Recent efforts have been made to explore how septal ACh modulates intrinsic GC firing (Pabst et al., 2016), and its role in memory formation (Raza et al., 2017). However, it remains unknown whether the processing of afferent inputs in the DG microcircuit is changed upon cholinergic modulation. We provide evidence for a cholinergic dynamic reconfiguration of the DG network induced by a nicotinic dependent feedforward perisomatic disinhibition of mature GCs, which potentiates responses to afferent inputs. The results presented here shed light on the mechanisms that permit a dynamic adaptation of processing and plasticity upon modulatory states.

RESULTS

Acetylcholine differentially affects immature and mature granule cells

To examine how ACh affects processing of afferent inputs in mature and immature 4 weeks old GCs (mat-GCs and 4wpi-GCs, respectively), we performed electrophysiological loose-patch recordings in mouse hippocampal slices to obtain activation profiles of individual GCs, while electrically stimulating the medial perforant pathway (mPP, Figure 1a). The cholinergic agonist carbamylcholine (carbachol, CBC) was bath applied to study the effect of a high acetylcholine (ACh) neuromodulatory state on the observed activation

profiles. We adjusted the intensity of the stimulus delivered to mPP at the threshold of each GC, i.e. an intensity that elicited GC spiking with 50% probability. Five trains of 10 pulses were delivered to the mPP at 1, 10, 20, and 40 Hz for each cell. Adult-born GCs were labeled by injecting a retrovirus in the dorsal DG that led to the expression of RFP or GFP in dividing cells, and acute hippocampal slices were prepared 4 weeks post retroviral injection (4 wpi). As we have previously shown (Pardi et al., 2015), the average number of spikes in response to mPP stimulation in control conditions decreases as stimulation frequency increases (Figure 1b, c), with a more drastic effect observed in mat-GCs, indicating that dentate GC have frequency filters with variable gain depending on their age (Pardi et al., 2015). Nevertheless, CBC induced a strong enhancement of the responses at high frequencies, specifically in mat-GCs, changing the filter properties of this population of GCs. This effect was more variable in 4wpi-GCs and CBC did not significantly change the responses of 4wpi-GCs to afferent stimulation (Figure 1c).

As mature neurons represent more than 95% of the total population of GCs in the adult DG, we hypothesized that the effect of CBC would also impact on the collective spiking of the GC population. Because the biggest effect in individual neurons was observed upon 10 Hz stimulation of the mPP, we studied the mechanisms of action of the cholinergic modulation at this frequency. This frequency is physiologically relevant, since the DG predominantly oscillates at frequencies near 10Hz in vivo (Jung and McNaughton, 1993, Leutgeb et al., 2007, Neunuebel and Knierim, 2012), and the medial septum is involved in the generation of these oscillations (Carpenter et al., 2017, Kang et al., 2017).

Population spike (pop spike, PS) responses were obtained by placing an extracellular electrode in the GCL of the DG, and stimulating the mPP fibers with trains of 10 pulses at 10 Hz (Figure 1d). Consistent with loose-patch recordings, pop spike amplitude in control conditions decreased strongly along the pulses of the stimulation train, as there are less GCs that respond at the last pulses (Figure 1d). As expected, bath application of CBC produced an increase in the pop spike responses to afferent stimuli at 10 Hz in the GCL (Figure 1e). Importantly, the increase in GCs activity is transferred postsynaptically, since we observed a concomitant significant increase in the activity of CA3 (Figure S1).

To better control the spatial and temporal release of ACh, we explored if endogenous release of ACh from septal axons would produce a similar increase in the activity of the DG. For this, we used the double transgenic mouse line ChAT-ChR2, which expresses the photoactivatable protein channelrhodopsin-2 in all cholinergic neurons. We obtained hippocampal slices from these animals, and elicited endogenous release of ACh from cholinergic terminals stimulating with blue light (Figure 2a). We recorded pop spikes in response to mPP stimulation before and after the blue-light illumination protocol (5-seconds trains of light pulses at 20 Hz delivered every minute, paired with electrical activation of mPP, Figure S2). Endogenous ACh release also augmented the pop spike responses in the DG upon 10 Hz electrical stimulation of mPP compared to the control condition before illumination (Figure 2c). The average gain in activation was 1.33 ± 0.06, and it was more prominent at the initial pulses (1.57 ± 0.14), but also significant for the last pulses of the train (Figure 2d). This neuromodulatory gain, thus, allows GCs to follow a wider frequency range of afferent stimuli.

To confirm that this cholinergic modulation was due to activation of septal cholinergic terminals, we performed stereotaxic injections of an adenovirus carrying the floxed version of ChR2 (AAV9-DIO-ChR2) delivered to the medial septum of $ChAT^{Cre}$ mice. In slices obtained from these animals, pairing optogenetic activation of septal cholinergic terminals with afferent activation also induced an increase in the pop spike response (Figure S3).

In order to verify that the modulation of mat-GCs´ activity is indeed cholinergic, we pharmacologically blocked ACh receptors with different antagonists. We used broad spectrum antagonists for both muscarinic (atropine) and nicotinic (mecamylamine) receptors. As expected for a cholinergic modulation, perfusion with ACSF containing these antagonists prevented the optogenetically induced potentiation of GC responses (Figure 2 e). Interestingly, bath application of atropine alone was insufficient to block the cholinergic neuromodulatory effects, suggesting that nicotinic receptors are primarily involved in the signaling pathway.

Activation of mPP not only generates excitation but it also recruits inhibitory circuits that regulate the activation of GCs (Marín-Burgin et al., 2012). We hypothesized that the increase in the amplitude of the pop spike upon cholinergic activation could be generated by an increase in the excitatory inputs, a decrease in the inhibitory inputs or a change in the intrinsic properties of the neurons. To explore the underlying mechanism, we first evaluated the involvement of inhibitory circuits by pharmacologically blocking $GABA_A$ receptors with picrotoxin (Figure 3a). In this condition, optogenetic activation of cholinergic terminals in the DG did not induce a potentiation of the pop spike response, indicating that cholinergic neuromodulation requires intact inhibitory circuits (Figure 3b-d). This result also suggests that cholinergic modulation does not involve a change in excitation.

Last, to evaluate if the effect of cholinergic modulation was due to a change in the intrinsic properties of the neurons, we measured the resting membrane potential (Vm), the action potential threshold and the input resistance (IR) of neurons upon activation of cholinergic inputs. Although CBC induced a small depolarization of the neuronal membrane potential as previously reported (Muller et al., 1988), the endogenous release of ACh did not affect Vm, the threshold or the IR of the recorded neurons (RMP -76.53 ± 2.03 vs -76.13 ± 3.37; IR 522.3 ± 58.46 vs 579.4 ± 42.59; threshold -40.2 ± 2.05 vs -42.2 ± 1.67, ns paired t-test, N=7), further suggesting that the increased responses of neurons upon cholinergic modulation is not explained by a modification of the intrinsic cell properties, but presumably due to a modulation of the inhibitory circuits.

Synaptic mechanisms underlying cholinergic modulation of granule cells

Because blocking inhibitory circuits prevents the cholinergic-induced increase in activity of GCs, we investigated the precise contribution of the evoked excitatory and inhibitory inputs to GCs at different modulatory states. We performed whole-cell voltage-clamp recordings of mat-GCs to measure excitatory and inhibitory responses elicited at 10 Hz stimulation of mPP axons in hippocampal slices from ChAT-ChR2 mice (Figure 4a). In this

configuration, we isolated inhibitory postsynaptic currents (IPSCs) or excitatory postsynaptic currents (EPSCs) by clamping the voltage of the neuron at the reversal potential of excitation (0mV) or inhibition (-60mV), respectively (Figure 4b). As expected, combining optogenetic release of endogenous ACh with activation of mPP induced a slow but strong, long lasting decrease in the IPSC, whereas EPSC was largely unaffected by cholinergic activation (Figure 4c, d). This produced an increase in the E/I balance of neurons that explains the changes in the activity profile (Figure 4 e). Because different ACh receptors are known to be expressed in both GCs and interneurons, the overall effect could be a combination of multiple pathways activated in different cell types. In agreement with our results at the population level, bath application of the nonspecific nicotinic antagonist mecamylamine prevented the light-evoked reduction in the IPSC (Figure 4 f), confirming the crucial role of nicotinic receptors in the cholinergic modulation of the DG activity.

Taken together, these results demonstrate that activation of cholinergic terminals in the DG selectively suppresses inhibitory inputs onto mat-GC recruited by activation of mPP. Thus, the resulting increase in the E/I balance of these neurons can explain their stronger spiking response to afferent inputs.

Acetylcholine specifically reduces the feedforward and perisomatic components of evoked IPSCs in granule cells

Because ACh release produces a very strong effect on evoked inhibition onto mat-GCs, we further explored which specific component of this inhibition is affected. As previously mentioned, activation of mPP not only produces excitation on GCs but also activates inhibitory circuits in a feedforward manner (Marín-Burgin et al., 2012). In addition, activation of GCs can also recruit feedback inhibition onto themselves and others, and this inhibition can influence their activity, especially during trains of stimuli (Roux and Buzsaki, 2015). These two types of inhibition are known to exert different functions in shaping the firing patterns of principal neurons. To study the specific regulation of feedforward

inhibition by ACh, we pharmacologically blocked the output of the DG GCs by bath application of DCGIV (Figure 5a), an agonist of group II metabotropic glutamate receptors ($mGluR_{2/3}$) that reduces release probability in mossy fiber terminals (Kamiya et al., 1996). Application of DCGIV abolishes feedback inhibition, and the remaining inhibition correspons then to feedforward inhibition (IPSC-FF). In this condition, whole-cell voltage-clamp experiments were performed in mat-GCs upon stimulation of mPP, before and after optogenetic release of ACh (Figure 5b). Cholinergic modulation strongly reduced the FF component of the IPSC (Figure 5c).

Conversely, to assess the feedback component of the IPSC, we placed the stimulating electrode directly in the GCL, electrically activating GCs that recruit feedback inhibition (IPSC-FB) onto other GCs, and thus bypassing the mPP axonal activation (Figure 5d). Surprisingly, the FB component is unaffected by cholinergic modulation (Figure 5 e-f). These results indicate that ACh can specifically decrease the feedforward inhibitory component recruited onto GCs upon mPP activation.

To further dissect the spatial contribution of inhibition that is affected by ACh, we isolated perisomatic and dendritic inhibition by placing a stimulating electrode either in the granule cell layer (GCL) or in the molecular layer, respectively (Figure 5g). Interestingly, we found that direct perisomatic inhibition was very strongly reduced by endogenous ACh release, while dendritic inhibition was less affected (Figure 5h) and thus the perisomatic/dendritic IPSC ratio was largely reduced (Figure 5i), suggesting a spatial reorganization of inhibition.

Acetylcholine strongly reduces PVIs but not SOMIs elicited IPSCs in granule cells

The reduction of specific components of inhibition by ACh suggests that its effect might be mediated by a specific subpopulation of inhibitory interneurons. As previously mentioned, synaptic inhibition is provided by two main interneuron types in the hippocampus, PVIs and SOMIs (Freund and Buzsaki, 1996, Rudy et al., 2011, Yuan et al., 2017). PVIs provide

powerful feedforward and feedback inhibition to large populations of GCs in the perisomatic region (Sambandan et al., 2010), while SOMIs are classically studied as dendritic targeting interneurons that participate more strongly in feedback inhibition, although it has been recently shown that they can be divided in functionally distinct subpopulations of SOMIs (Yuan et al., 2017). Because PVIs but not SOMIs are the main FF inhibitory population in the DG (Hosp et al., 2014, Savanthrapadian et al., 2014), we hypothesized that ACh might act differentially on these two populations of interneurons.

In order to specifically assess the role of ACh in PVI-to-GC inhibition, a Cre-inducible AAV vector carrying ChR2 (AAV-DIO-ChR2) was stereotaxically injected in the DG of PV-Cre animals. We obtained hippocampal slices from these animals, in which we optogenetically activated PVI (Figure 6a). We delivered light trains of 10 pulses at 10 Hz (PW = 5ms), while recording the evoked IPSCs in mat-GCs using patch-clamp whole-cell recordings at the reversal potential of excitation (0mV). Consistent with the main role of PVIs in the feedforward inhibitory circuit of the DG, IPSCs induced on GCs by activation of PVIs are strongly reduced by bath application of CBC (Figure 6b, c). Interestingly, when we studied the effect of CBC onto SOMI-elicited-IPSCs (by injecting AAV-DIO-ChR2 in the DG of SOM-Cre animals, Figure 6d), the recorded IPSCs were not affected (Figure 6e, f), suggesting that ACh selectively reduces PVI-mediated inhibition onto GCs.

Acetylcholine shifts the evoked E/I balance of PVIs and SOMIs in opposite directions

Because PVIs are recruited by mPP axons to produce feedforward inhibition, we further explored how that population of neurons processed afferent inputs upon cholinergic modulation. We performed whole-cell voltage-clamp recordings of PVIs to measure excitatory and inhibitory responses elicited at 10 Hz stimulation of the mPP (Figure 7a, b). Remarkably, in addition to the reduction of direct inhibition from PVIs to GCs by release of ACh, CBC produced a powerful decrease in the E/I balance of PVIs in response to mPP activation (Figure 7 c, d). The stronger inhibition received by PVIs (Figure 7c) upon cholinergic modulation suggests that another population of interneurons should be more

active in this modulatory state. Because a subpopulation of SOMIs are known to inhibit PVIs (Yuan et al., 2017), we then performed whole-cell voltage-clamp recordings of hilar SOMIs to measure excitatory and inhibitory responses elicited by stimulation of the mPP (Figure 7e, f). Strikingly, CBC produced an increase in the E/I balance of SOMIs (Figure 7g, h), suggesting that these interneurons are more active during a cholinergic neuromodulatory state. Notably, the evoked IPSC onto SOMIs changed in an opposite direction compared to PVIs, suggesting that cholinergic modulation reconfigures inhibitory microcircuits shifting the relative contribution of different populations of interneurons that in turn control the DG activity.

High-frequency stimulation produces LTP in the DG when paired with activation of cholinergic terminals

What is the functional consequence of the observed reconfiguration of inhibition? One possibility is that by disinhibiting GCs, ACh could produce a temporal window to allow plasticity in an otherwise very sparsely active region. We tested this hypothesis by using a tetanic stimulation protocol on hippocampal slices (Figure 8a). Importantly, this stimulation protocol is insufficient to produce LTP on mat-GCs unless inhibitory circuits are blocked (Snyder et al., 2001). We recorded the slope of the field excitatory postsynaptic potential (fEPSP) in slices obtained from ChAT-ChR2 mice, before and after tetanic stimulation (Figure 8b). As previously reported, this high frequency stimulation (HFS) was insufficient to produce a potentiation of the response, consistent with the fact that the vast majority of the DG GCs are mature. Remarkably, in the same slices we were able to induce LTP if we paired tetanic stimulation with endogenous release of ACh (Figure 8c). These results indicate that ACh can lower LTP-induction thresholds in the DG, providing a temporal window in which incoming inputs are able to induce long term synaptic changes. Interestingly, the same amount of activation of cholinergic terminals does not induce LTP if low-frequency stimuli are delivered to the mPP, indicating that ACh could act as a selective amplifier for high frequency inputs (Figure 8d, e).

DISCUSSION

In the present work, we showed that endogenous ACh release into the DG produced an increased activation of mat-GCs in response to afferent stimuli, without changing the activation of immature GCs. The increased response is due to a highly precise reconfiguration of inhibitory circuits that results in a disinhibition of GCs, creating a window of opportunity for plasticity. In accordance with this, coincident activation of afferent perforant path inputs with ACh release produced a long-term-potentiated response in GCs.

The difference in the cholinergic effect on mature and immature GCs can be explained by the fact that immature neurons have underdeveloped perisomatic feedforward inhibition (Marín-Burgin et al., 2012), which is the main target of the cholinergic effects. The cholinergic system is then able to independently modulate the input processing properties of the mat-GC population, without interfering with the parallel processing of the sub-population of immature neurons.

Our results show a highly specific reconfiguration of inhibitory microcircuits, producing opposite effects in different subpopulations of genetically defined interneurons. We observed a nicotinic-dependent reduction of evoked feedforward inhibition in mat-GCs. In the DG, this type of inhibition is primarily carried out by PVIs (Zipp et al., 1989, Sambandan et al., 2010), which indeed received more inhibition under cholinergic modulation and produced less direct inhibition onto mat-GCs. Cholinergic reduction of inhibition has also been observed in CA1, where inhibition from PVIs to pyramidal neurons is reduced by ACh through nicotinic receptors (Tang et al., 2011), suggesting a common mechanism of cholinergic-mediated disinhibition in the hippocampus.

Previous studies have shown a strong nicotinic mediated depolarization of hilar interneurons whose dendritic trees are within the hilus (Pabst et al., 2016). Hilar interneurons, including one subgroup of SOMI, are known to inhibit PVI (Yuan et al.,

2017), being able to mediate the observed disinhibitory effect. Upon cholinergic modulation, we found an increase in the E/I balance of hillar SOMIs in response to afferent stimulation, which supports these neurons as good candidates for mediating the disinhibitory effect on mat-GCs. In fact, optogenetic activation of a subgroup of SOMIs in CA1 subregion was shown to disinhibit Schaffer collaterals inputs to pyramidal cells and increase the magnitude of LTP in this region (Leao et al., 2012).

The synaptic location of inhibition has important consequences for neuronal computations, since somatic inhibition modulates the gain (division effect) and dendritic inhibition have a subtractive effect (Pouille et al., 2013). The independent modulation of perisomatic and dendritic inhibition could presumably produce very different outputs of neuronal processing. Interestingly, *in vivo* studies have shown that inhibition at GC somata (presumably by PVIs) is reduced during exploratory movement, when ACh levels are high, whereas inhibition in the dendrites might be increased (Paulsen and Moser, 1998); These apparently contradictory changes could together act as filter and amplifier, increasing the contrast between signals with different relations to ongoing behavior (Paulsen and Moser, 1998). In this scenario, weak inputs would not be able to bypass the strong dendritic inhibition, but once they do, they are amplified by a reduced perisomatic inhibition. Our results are compatible with this model, in which we observed that the relative contribution of PVI-mediated perisomatic inhibition is reduced in comparison with dendritic inhibition, very likely carried by SOMIs. In fact, a number of studies propose a main role for ACh in increasing the signal to noise ratio (Hasselmo, 2006).

The architecture of inhibitory subcircuits ensures richness in the possible dynamics within networks of principal neurons (Isaacson and Scanziani, 2011, Hu et al., 2014, Kepecs and Fishell, 2014). Through neuromodulation, different populations of interneurons can serve to gate information flow within the DG in specific behavioral events. It has been reported that LTP is more easily induced in the DG during exploration of novel environments, where ACh levels are high (Davis et al., 2004). Furthermore, Fos expression in the DG is greater after novel context exploration (VanElzakker et al., 2008). In the present work, we showed that pairing brief optogenetic activation of cholinergic fibers with stimulation of afferent

inputs was sufficient to produce a strong, long-lasting potentiation of the mPP-GC pathway. Because this potentiation requires more than one pulse of afferent stimulation, the cholinergic-DG system might serve to filter out temporally sparse inputs, conveying specificity and at the same time allowing high frequency inputs to produce long-term synaptic changes, thus increasing the signal to noise ratio of the circuit. This phenomenon is compatible with the phasic acetylcholine release in the hippocampus found during performance on a working memory task, where it is associated with the reward delivery, novelty, or fear (Marrosu et al., 1995, Acquas et al., 1996, Teles-Grilo Ruivo et al., 2017). In addition, recent experiments using optogenetic release of ACh in the DG have shown an increase in associative fear memory in animals preexposed to a spatial context in the presence of ACh, suggesting that novelty-induced ACh release primes future contextual associations (Hersman et al., 2017).

The present work provides a circuit mechanism by which ACh dynamically reconfigures the DG network, allowing this brain region to change its information processing properties by shifting the relative contribution of different subpopulations of interneurons. These changes favor the induction of long-term synaptic plasticity, essential for memory formation, and can serve *in vivo* to adapt the encoding to the behavioral and cognitive demands of different tasks. Understanding the role of cholinergic modulation of input processing in the hippocampus can have important implications for neurodegenerative diseases in which the cholinergic and consequently the memory systems are severely impaired as observed in Alzheimer´s disease (Ballinger et al., 2016).

ACKNOWLEDGEMENTS

We thank members of the Marin-Burgin lab, the Refojo lab and Muraro lab for insightful discussions. We thank Jens Bruening for sharing Ai27 mice with us. We thank Hillel Adesnik for his valuable comments on the manuscript. This work was supported by grants

from the Argentine Agency for the Promotion of Science and Technology (PICT2013-0182 and PICT2015-0364), ECOS 2014 to AMB and FOCEM-Mercosur (COF 03/11).

MATERIALS AND METHODS

Viral vectors preparation

A replication-deficient retroviral vector based on the Moloney murine leukemia virus was used to express RFP or GFP under a CAG promoter as previously described (Marín-Burgin et al., 2012). Retroviral particles were assembled using three separate plasmids containing the capside (CMV-vsvg), viral proteins (CMV-gag/pol), and the transgene (CAG-RFP or CAG-GFP). Plasmids were transfected onto HEK 293T cells using deacylated polyethylenimine. Virus-containing supernatant was harvested 48 hr after transfection and concentrated by two rounds of ultracentrifugation. Virus titer was typically $\sim 10^5$ particles/µl.

Animals and surgery for viral delivery

For the neurogenesis experiments, female C57Bl/6J mice 6–8 weeks of age were housed at 4 mice per cage, with one running wheel. Running wheel housing started 2–4 days before surgery and continued until the day of slice preparation. For surgery, mice were anesthetized (150 µg ketamine/15 µg xylazine in 10 µl saline/g), and virus (1 µl at 0.125 µl/min) was infused into the dorsal area of the right DG using sterile microcapillary calibrated pipettes and stereotaxic references (coordinates from bregma: −2 mmanteroposterior,-1.5 mm lateral, -1.9 mm ventral). Animals were killed for acute slice preparation 4 weeks after the surgery.

For optogenetic experiments with interneurons, PV^{Cre} or SOM^{Cre} mice 8–20 weeks of age were anesthetized (150 µg ketamine/15 µg xylazine in 10 µl saline/g), and AAV9-EF1a-double floxed-hChR2(H134R)-mCherry-WPRE-HGHpA (AAV-DIO-ChR2) virus (0.5 µl at 0.125 µl/min) was infused into the dorsal area of the right DG using sterile microcapillary calibrated pipettes and stereotaxic references (same coordinates as before). Animals were killed for acute slice preparation 2-6 weeks after the surgery.

For optogenetic activation of septal cholinergic fibers in the DG, $ChAT^{Cre}$ mice 8-16 weeks of age were anesthetized (150 µg ketamine/15 µg xylazine in 10 µl saline/g), and AAV-DIO-ChR2 virus (1 µl at 0.125 µl/min) was infused into the medial septum using sterile microcapillary calibrated pipettes and stereotaxic references (coordinates from bregma: 0.9 mm anteroposterior, 0.0 mm lateral, -3.6 mm ventral). Animals were killed for acute slice preparation 2-6 weeks after the surgery.

To generate *$Pvalb^{Cre}$*;$CAG^{FloxStopTom}$ (PV-Tom) mice, *B6;129P2-Pvalbtm1(cre)Arbr/J (PV^{Cre})* mice (Hippenmeyer et al., 2005) were crossed to *B6.Cg-Gt(ROSA)26Sortm14(CAG-tdTomato)Hze/J (Ai14)* conditional reporter mice. Animals heterozygous for Cre were used.

To generate *SOM^{Cre}*;$CAG^{FloxStopTom}$ (SOM-Tom) mice, *Sttm2.1(cre)Zjh/J (SOM^{Cre})* were crossed to *B6.Cg-Gt(ROSA)26Sortm14(CAG-tdTomato)Hze/J (Ai14)* conditional reporter mice. Animals heterozygous for Cre were used.

To generate *$ChAT^{Cre}$*;Ai27 (ChAT-ChR2) mice, *B6;129S6-Chattm2(cre)Lowl/J($ChAT^{cre}$)* mice were crossed to *B6.Cg-Gt(ROSA)26Sortm27.1(CAG-COP4*H134R/tdTomato)Hze/J (Ai27)* conditional channelrhodopsin mice. Animals heterozygous for Cre were used.

Experimental protocols were approved by the Institutional Animal Care and Use Committee of the Faculty of Science from the University of Buenos Aires (Protocols Number 52) according to the Principles for Biomedical Research involving animals of the Council for International Organizations for Medical Sciences and provisions stated in the Guide for the Care and Use of Laboratory Animals.

Slice preparation

Mice were anesthetized and decapitated. Brains were removed into a chilled solution containing (mM) 110 choline-Cl^-, 2.5 KCl, 2.0 NaH_2PO_4, 25 $NaHCO_3$, 0.5 $CaCl_2$, 7 $MgCl_2$, 20 dextrose, 1.3 Na^+-ascorbate, 3.1 Na^+-pyruvate. The right hippocampus was dissected and slices (400 µm thick) were cut transversally to the longitudinal axis in a vibratome and transferred to a chamber containing artificial cerebrospinal fluid (ACSF; mM): 125 NaCl, 2.5 KCl, 2.3 NaH_2PO_4, 25 $NaHCO_3$, 2 $CaCl_2$, 1.3 $MgCl_2$, 1.3 Na^+-ascorbate, 3.1 Na^+-pyruvate,

and 10 dextrose (315 mOsm). Slices were bubbled with 95% O_2/5% CO_2 and maintained at 30°C for approximately 1 hr before experiments started. Salts were acquired from Sigma-Aldrich (St. Louis, MO). When carbamoycholine chloride (CBC, 5-20 µM, Sigma Aldrich), atropine (10 µM, Sigma Aldrich), mecamylamine (20 µM, ABCAM), picrotoxine (PTX, 100 µM, Sigma Aldrich), were used, they were perfused into the bath solution.

Extracellular recordings

A field-recording microelectrode was placed on the granule cell layer (GCL) or molecular layer (ML) to record the pop spike or the fEPSP, respectively, in response to the mPP stimulation. The input strength was adjusted to elicit pop spike responses between 0.5 and 2 mV or fEPSP responses between -0.15 and -0.6 mV/ms, within the linear part of the dynamic range of responses. For a given input strength within a slice, the number of mPP axons stimulated in control conditions or after neuromodulatory manipulations were the same.

Electrophysiological single cell recordings

Recorded neurons were visually identified by fluorescence and infrared DIC video microscopy. The mature neuronal population encompassed RFP^- or GFP^- neurons localized in the outer third of the GCL (Mongiat et al., 2009). Whole-cell recordings were performed using microelectrodes (4–5 MΩ) filled with (in mM) 130 CsOH, 130 D-gluconic acid, 2 $MgCl_2$, 0.2 EGTA, 5 NaCl, 10 HEPES, 4 ATP-tris, 0.3 GTP-tris, 10 phosphocreatine. In experiments where the intrinsic responses to current pulses were evaluated, a potassium gluconate internal solution was used (in mM): 120 potassium gluconate, 4 $MgCl_2$, 10 HEPES buffer, 0.1 EGTA, 5 NaCl, 20 KCl, 4 ATP-tris, 0.3 GTP-tris, and 10 phosphocreatine (pH = 7.3; 290 mOsm). In experiments where the perisomatic and dendritic inhibitory responses were evaluated, a CsOH with symmetric cloride internal solution was used (in mM): 140 CsCl, 2 MgCl2, 0.1 EGTA, 5 NaCl, 10 HEPES, 4 ATP-tris, 0.3 GTP-tris, 10 phosphocreatine (pH = 7.3; 290 mOsm).Loose-patch recordings were performed with ACSF-filled patch pipettes (5–6 MΩ). Field recordings were performed using patch pipettes

(5 MΩ) filled with 3 M NaCl. Recordings were obtained using Multiclamp 700B amplifiers, (Molecular Devices, Sunnyvale, CA), digitized, and acquired at 20 KHz onto a personal computer using the pClamp10 software. Membrane capacitance and input resistance were obtained from current traces evoked by a hyperpolarizing step of 10 mV. Series resistance was typically 10–20 MΩ, and experiments were discarded if higher than 40 MΩ.

Evoked postsynaptic currents and conductance

Evoked monosynaptic excitatory postsynaptic currents (EPSC) and inhibitory postsynaptic currents (IPSC) were recorded after stimulation. EPSCs were isolated by voltage clamping GC, PVI or SOMI at the reversal potential of the IPSC measured for each individual neuron (~60 mV). In turn, IPSCs were recorded at the reversal potential of the EPSC (~0 mV). When present, direct monosynaptic IPSC elicited in presence of kynurenic acid (KYN, Sigma Aldrich) was subtracted from the total IPSC. Synaptic excitatory and inhibitory conductances were computed as the EPSC or IPSC divided by the driving force at which the synaptic currents were recorded.

Measurement of feedforward and feedback inhibition

To dissect feedforward component of the inhibitory response, the stimulating electrode was placed on the mPP, while mossy fiber synapses were blocked with DCGIV (1 µM, Tocris)(Kamiya et al., 1996). In this condition, the remaining feedforward current was measured, before and after the optogenetic stimulating protocol, always in presence of DCGIV. In order to isolate the feedback component of the inhibitory response, the stimulating electrode was placed directly on the GCL. When present, direct monosynaptic IPSC recorded in KYN was subtracted from the IPSC.

Characterization of direct perisomatic and dendritic inhibition

To dissect dendritic component of the inhibitory response, stimulating electrodes were placed in the granule cell layer (GCL) and the molecular layer (ML) to activate monosynaptic perisomatic or dendritic inhibition. Experiments were performed in the

presence of 6 mM kynurenic acid (Kyn) to block glutamatergic transmission. IPSCs were subsequently measured in whole-cell recordings from individual cells. In this conditions, perisomatic IPSCs display a reversal potential of ~0 mV due to the recording conditions under symmetrical Cl^-, while dendritic IPSCs display a positive driving force at that potential.

Optogenetics

Hippocampal slices containing ChR2 expressed either in cholinergic fibers or interneurons were obtained. ChR2 expressing neurons or axons were stimulated using a 470 nm LED source delivered through the epifluorescence pathway of the upright microscope (63X objective for whole-cell recordings, 20X for field recordings) commanded by the acquisition software. For cholinergic neuromodulatory experiments in slices obtained from ChAT-ChR2 mice, 5 to 10 trains of blue light (20Hz, pulse width 10 ms) were delivered for 5 seconds every minute. Within the light train, either a single pulse or a train of 10 pulses at 10 Hz was delivered to the stimulating electrode (pulse width 0.2ms) so that the onset of the light pulse was coincident with the electrical stimulation. Cholinergic modulation slowly augmented the amplitude of pop spikes until reaching a plateau at around 10 minutes (Figure S2). We then measured the responses before and 15 minutes after the beginning of the light stimulation protocol. Both the control and the neuromodulated experimental groups were measured in the absence of light and at the same intensity of mPP stimulation, in order to compare two identically stimulated conditions.

In other experiments, slices were obtained from $ChAT^{Cre}$ mice injected with the adeoviral vector AAV-DIO-ChR2 in the medial septum. 2-6 weeks after surgery, hippocampal slices were obtained from these animals and septal cholinergic axons in the DG were stimulated with blue light. For these experiments, light trains of 50 seconds were delivered to the preparation. At the onset of the light train (second 23), a train of 10 pulses of electrical stimulation was delivered at 10 Hz. Both the control and the neuromodulated

experimental groups were measured in the absence of light, in order to compare two identically stimulated conditions.

For optogenetic activation of interneuron populations, PV-Cre or SOM-Cre animals were injected with AAV-DIO-ChR2 in the dorsal DG in order to express ChR2 specifically in either subpopulation of interneurons. Light trains of 10 pulses at 10 Hz (pulse width 1-5 ms) were delivered every minute. The intensity of the light was adjusted in order to have a non-saturating evoked IPSC.

Statistical analysis

Unless otherwise specified, data are presented as mean ± SEM. Normality was assessed using Shapiro-Wilk's test, D'Agostino & Pearson omnibus test, or Kolmogórov-Smirnov's test, at a *p* value of 0.05. For normal distributions, homoscedasticity was assessed using Bartlett's test and F-test, at a *p* value of 0.05. For homogeneous variances, two-tailed ordinary or paired t-test was used for single comparisons, and ordinary or repeated measures ANOVA.

REFERENCES

Acquas E, Wilson C, Fibiger HC (1996) Conditioned and unconditioned stimuli increase frontal cortical and hippocampal acetylcholine release: effects of novelty, habituation, and fear. J Neurosci 16:3089-3096.

Andersen P, Bliss TV, Skrede KK (1971) Lamellar organization of hippocampal pathways. Exp Brain Res 13:222-238.

Bakker A, Kirwan CB, Miller M, Stark CE (2008) Pattern separation in the human hippocampal CA3 and dentate gyrus. Science 319.

Ballinger EC, Ananth M, Talmage DA, Role LW (2016) Basal Forebrain Cholinergic Circuits and Signaling in Cognition and Cognitive Decline. Neuron 91:1199-1218.

Bartos M, Vida I, Jonas P (2007) Synaptic mechanisms of synchronized gamma oscillations in inhibitory interneuron networks. Nat Rev Neurosci 8:45-56.

Bloem B, Poorthuis RB, Mansvelder HD (2014) Cholinergic modulation of the medial prefrontal cortex: the role of nicotinic receptors in attention and regulation of neuronal activity. Front Neural Circuits 8.

Burgess N, Maguire EA, O'Keefe J (2002) The human hippocampus and spatial and episodic memory. Neuron 35:625-641.

Carpenter F, Burgess N, Barry C (2017) Modulating medial septal cholinergic activity reduces medial entorhinal theta frequency without affecting speed or grid coding. Sci Rep 7:14573.

Danielson NB, Kaifosh P, Zaremba JD, Lovett-Barron M, Tsai J, Denny CA, Balough EM, Goldberg AR, Drew LJ, Hen R, Losonczy A, Kheirbek MA (2016) Distinct Contribution of Adult-Born Hippocampal Granule Cells to Context Encoding. Neuron 90:101-112.

Dannenberg H, Young K, Hasselmo M (2017) Modulation of Hippocampal Circuits by Muscarinic and Nicotinic Receptors. Front Neural Circuits 11:102.

Davis CD, Jones FL, Derrick BE (2004) Novel environments enhance the induction and maintenance of long-term potentiation in the dentate gyrus. J Neurosci 24:6497-6506.

Denny CA, Kheirbek MA, Alba EL, Tanaka KF, Brachman RA, Laughman KB, Tomm NK, Turi GF, Losonczy A, Hen R (2014) Hippocampal memory traces are differentially modulated by experience, time, and adult neurogenesis. Neuron 83:189-201.

Espósito MS, Piatti VC, Laplagne DA, Morgenstern NA, Ferrari CC, Pitossi FJ, Schinder AF (2005) Neuronal Differentiation in the Adult Hippocampus Recapitulates Embryonic Development. The Journal of Neuroscience 25:10074-10086.

Freund TF, Buzsaki G (1996) Interneurons of the hippocampus. Hippocampus 6:347-470.

Ge S, Yang CH, Hsu KS, Ming GL, Song H (2007) A critical period for enhanced synaptic plasticity in newly generated neurons of the adult brain. Neuron 54:559-566.

Haam J, Yakel JL (2017) Cholinergic modulation of the hippocampal region and memory function. J Neurochem 2:111-121.

Hasselmo ME (2006) The role of acetylcholine in learning and memory. Curr Opin Neurobiol 16:710-715.

Hasselmo ME, McGaughy J (2004) High acetylcholine levels set circuit dynamics for attention and encoding and low acetylcholine levels set dynamics for consolidation. Prog Brain Res 145:207-231.

Hersman S, Cushman J, Lemelson N, Wassum K, Lotfipour S, Fanselow MS (2017) Optogenetic excitation of cholinergic inputs to hippocampus primes future contextual fear associations. Sci Rep 7:017-02542.

Hosp JA, Struber M, Yanagawa Y, Obata K, Vida I, Jonas P, Bartos M (2014) Morpho-physiological criteria divide dentate gyrus interneurons into classes. Hippocampus 24:189-203.

Hu H, Gan J, Jonas P (2014) Interneurons. Fast-spiking, parvalbumin(+) GABAergic interneurons: from cellular design to microcircuit function. Science 345:31.

Isaacson Jeffry S, Scanziani M (2011) How Inhibition Shapes Cortical Activity. Neuron 72:231-243.

Jung MW, McNaughton BL (1993) Spatial selectivity of unit activity in the hippocampal granular layer. Hippocampus 3.

Kamiya H, Shinozaki H, Yamamoto C (1996) Activation of metabotropic glutamate receptor type 2/3 suppresses transmission at rat hippocampal mossy fibre synapses. J Physiol 493:447-455.

Kang D, Ding M, Topchiy I, Kocsis B (2017) Reciprocal Interactions between Medial Septum and Hippocampus in Theta Generation: Granger Causality Decomposition of Mixed Spike-Field Recordings. Front Neuroanat 11.

Kepecs A, Fishell G (2014) Interneuron cell types are fit to function. Nature 505:318-326.

Leao RN, Mikulovic S, Leao KE, Munguba H, Gezelius H, Enjin A, Patra K, Eriksson A, Loew LM, Tort AB, Kullander K (2012) OLM interneurons differentially modulate CA3 and entorhinal inputs to hippocampal CA1 neurons. Nature neuroscience 15:1524-1530.

Letzkus JJ, Wolff SB, Meyer EM, Tovote P, Courtin J, Herry C, Luthi A (2011) A disinhibitory microcircuit for associative fear learning in the auditory cortex. Nature 480:331-335.

Leutgeb JK, Leutgeb S, Moser MB, Moser EI (2007) Pattern separation in the dentate gyrus and CA3 of the hippocampus. Science 315:961-966.

Leutgeb S, Leutgeb JK, Moser MB, Moser EI (2005) Place cells, spatial maps and the population code for memory. Curr Opin Neurobiol 15:738-746.

Liu X, Ramirez S, Pang PT, Puryear CB, Govindarajan A, Deisseroth K, Tonegawa S (2012) Optogenetic stimulation of a hippocampal engram activates fear memory recall. Nature 484.

Lopez-Rojas J, Heine M, Kreutz MR (2016) Plasticity of intrinsic excitability in mature granule cells of the dentate gyrus. Sci Rep 6.

Lopez-Rojas J, Kreutz MR (2016) Mature granule cells of the dentate gyrus—Passive bystanders or principal performers in hippocampal function? Neuroscience & Biobehavioral Reviews 64:167-174.

Marín-Burgin A, Mongiat LA, Pardi MB, Schinder AF (2012) Unique Processing During a Period of High Excitation/Inhibition Balance in Adult-Born Neurons. Science 335:1238-1242.

Marin-Burgin A, Schinder AF (2012) Requirement of adult-born neurons for hippocampus-dependent learning. Behav Brain Res 227:391-399.

Marr D (1971) Simple memory: a theory for archicortex. Philos Trans R Soc Lond B Biol Sci 262.

Marrosu F, Portas C, Mascia MS, Casu MA, Fa M, Giagheddu M, Imperato A, Gessa GL (1995) Microdialysis measurement of cortical and hippocampal acetylcholine release during sleep-wake cycle in freely moving cats. Brain Res 671:329-332.

Mesulam MM, Mufson EJ, Wainer BH, Levey AI (1983) Central cholinergic pathways in the rat: An overview based on an alternative nomenclature (Ch1–Ch6). Neuroscience 10:1185-1201.

Mistry R, Dennis S, Frerking M, Mellor JR (2011) Dentate gyrus granule cell firing patterns can induce mossy fiber long-term potentiation in vitro. Hippocampus 21:1157-1168.

Mongiat LA, Esposito MS, Lombardi G, Schinder AF (2009) Reliable activation of immature neurons in the adult hippocampus. PLoS One 4:28.

Muller W, Misgeld U, Heinemann U (1988) Carbachol effects on hippocampal neurons in vitro: dependence on the rate of rise of carbachol tissue concentration. Exp Brain Res 72:287-298.

Nakashiba T, Cushman JD, Pelkey KA, Renaudineau S, Buhl DL, McHugh TJ (2012) Young dentate granule cells mediate pattern separation, whereas old granule cells facilitate pattern completion. Cell 149.

Neunuebel JP, Knierim JJ (2012) Spatial firing correlates of physiologically distinct cell types of the rat dentate gyrus. J Neurosci 32:3848-3858.

Neunuebel JP, Knierim JJ (2014) CA3 retrieves coherent representations from degraded input: direct evidence for CA3 pattern completion and dentate gyrus pattern separation. Neuron 81:416-427.

Nitz D, McNaughton B (2004) Differential modulation of CA1 and dentate gyrus interneurons during exploration of novel environments. J Neurophysiol 91:863-872.

Pabst M, Braganza O, Dannenberg H, Hu W, Pothmann L, Rosen J, Mody I, van Loo K, Deisseroth K, Becker AJ, Schoch S, Beck H (2016) Astrocyte Intermediaries of Septal Cholinergic Modulation in the Hippocampus. Neuron 90:853-865.

Palacios-Filardo J, Mellor JR (2018) Neuromodulation of hippocampal long-term synaptic plasticity. Curr Opin Neurobiol 54:37-43.

Pardi MB, Ogando MB, Schinder AF, Marin-Burgin A (2015) Differential inhibition onto developing and mature granule cells generates high-frequency filters with variable gain. eLife 11:08764.

Parikh V, Kozak R, Martinez V, Sarter M (2007) Prefrontal acetylcholine release controls cue detection on multiple timescales. Neuron 56:141-154.

Paulsen O, Moser EI (1998) A model of hippocampal memory encoding and retrieval: GABAergic control of synaptic plasticity. Trends Neurosci 21:273-278.

Pepeu G, Giovannini MG (2004) Changes in acetylcholine extracellular levels during cognitive processes. Learn Mem 11:21-27.

Pernia-Andrade AJ, Jonas P (2014) Theta-gamma-modulated synaptic currents in hippocampal granule cells in vivo define a mechanism for network oscillations. Neuron 81:140-152.

Pinto L, Goard MJ, Estandian D, Xu M, Kwan AC, Lee SH, Harrison TC, Feng G, Dan Y (2013) Fast modulation of visual perception by basal forebrain cholinergic neurons. Nature neuroscience 16:1857-1863.

Pouille F, Watkinson O, Scanziani M, Trevelyan AJ (2013) The contribution of synaptic location to inhibitory gain control in pyramidal cells. Physiological reports 1:e00067.

Prince LY, Bacon TJ, Tigaret CM, Mellor JR (2016) Neuromodulation of the Feedforward Dentate Gyrus-CA3 Microcircuit. Frontiers in Synaptic Neuroscience 8:32-32.

Ramirez S, Liu X, Lin PA, Suh J, Pignatelli M, Redondo RL, Ryan TJ, Tonegawa S (2013) Creating a false memory in the hippocampus. Science 341:387-391.

Raza SA, Albrecht A, Caliskan G, Muller B, Demiray YE, Ludewig S, Meis S, Faber N, Hartig R, Schraven B, Lessmann V, Schwegler H, Stork O (2017) HIPP neurons in the dentate gyrus mediate the cholinergic modulation of background context memory salience. Nat Commun 8:017-00205.

Roux L, Buzsaki G (2015) Tasks for inhibitory interneurons in intact brain circuits. Neuropharmacology 88:10-23.

Rudy B, Fishell G, Lee S, Hjerling-Leffler J (2011) Three groups of interneurons account for nearly 100% of neocortical GABAergic neurons. Dev Neurobiol 71:45-61.

Ryan TJ, Roy DS, Pignatelli M, Arons A, Tonegawa S (2015) Memory. Engram cells retain memory under retrograde amnesia. Science 348:1007-1013.

Sambandan S, Sauer JF, Vida I, Bartos M (2010) Associative plasticity at excitatory synapses facilitates recruitment of fast-spiking interneurons in the dentate gyrus. J Neurosci 30:11826-11837.

Sarter M, Hasselmo ME, Bruno JP, Givens B (2005) Unraveling the attentional functions of cortical cholinergic inputs: interactions between signal-driven and cognitive modulation of signal detection. Brain research Brain research reviews 48:98-111.

Sarter M, Parikh V, Howe WM (2009) Phasic acetylcholine release and the volume transmission hypothesis: time to move on. Nat Rev Neurosci 10:383-390.

Sasaki T, Piatti VC, Hwaun E, Ahmadi S, Lisman JE, Leutgeb S, Leutgeb JK (2018) Dentate network activity is necessary for spatial working memory by supporting CA3 sharp-wave ripple generation and prospective firing of CA3 neurons. Nature neuroscience 21:258-269.

Savanthrapadian S, Meyer T, Elgueta C, Booker SA, Vida I, Bartos M (2014) Synaptic properties of SOM- and CCK-expressing cells in dentate gyrus interneuron networks. J Neurosci 34:8197-8209.

Snyder JS, Kee N, Wojtowicz JM (2001) Effects of adult neurogenesis on synaptic plasticity in the rat dentate gyrus. J Neurophysiol 85:2423-2431.

Stone SS, Teixeira CM, Zaslavsky K, Wheeler AL, Martinez-Canabal A, Wang AH, Sakaguchi M, Lozano AM, Frankland PW (2011) Functional convergence of developmentally and adult-generated granule cells in dentate gyrus circuits supporting hippocampus-dependent memory. Hippocampus 21:1348-1362.

Struber M, Sauer JF, Jonas P, Bartos M (2017) Distance-dependent inhibition facilitates focality of gamma oscillations in the dentate gyrus. Nat Commun 8:017-00936.

Tang AH, Karson MA, Nagode DA, McIntosh JM, Uebele VN, Renger JJ, Klugmann M, Milner TA, Alger BE (2011) Nerve terminal nicotinic acetylcholine receptors initiate quantal GABA release from perisomatic interneurons by activating axonal T-type (Cav3) Ca(2)(+) channels and Ca(2)(+) release from stores. J Neurosci 31:13546-13561.

Teles-Grilo Ruivo LM, Baker KL, Conway MW, Kinsley PJ, Gilmour G, Phillips KG, Isaac JTR, Lowry JP, Mellor JR (2017) Coordinated Acetylcholine Release in Prefrontal Cortex and Hippocampus Is Associated with Arousal and Reward on Distinct Timescales. Cell Rep 18:905-917.

Tronel S, Charrier V, Sage C, Maitre M, Leste-Lasserre T, Abrous DN (2015) Adult-born dentate neurons are recruited in both spatial memory encoding and retrieval. Hippocampus 25:1472-1479.

van Praag H, Schinder AF, Christie BR, Toni N, Palmer TD, Gage FH (2002) Functional neurogenesis in the adult hippocampus. Nature 415:1030-1034.

VanElzakker M, Fevurly RD, Breindel T, Spencer RL (2008) Environmental novelty is associated with a selective increase in Fos expression in the output elements of the hippocampal formation and the perirhinal cortex. Learn Mem 15:899-908.

Wainer B, Levey A, Rye D, Mesulam M, Mufson E (1985) Cholinergic and non-cholinergic septohippocampal pathways. Neurosci lett 54:45-52.

Yuan M, Meyer T, Benkowitz C, Savanthrapadian S, Ansel-Bollepalli L, Foggetti A, Wulff P, Alcami P, Elgueta C, Bartos M (2017) Somatostatin-positive interneurons in the dentate gyrus of mice provide local- and long-range septal synaptic inhibition. eLife 3:21105.

Zipp F, Nitsch R, Soriano E, Frotscher M (1989) Entorhinal fibers form synaptic contacts on parvalbumin-immunoreactive neurons in the rat fascia dentata. Brain Res 495:161-166.

FIGURE LEGENDS

Figure 1. Carbachol increases the spiking response of mature GCs.

a. Experimental design. The image shows a hippocampus slice with 4-weeks-old GC (4wpiGC) expressing RFP. Scale bar: 50 µm. The upper timeline indicates the time of retroviral injection. Right: The scheme shows the recording configuration: a stimulating electrode was placed in the medial perforant path (mPP) to deliver 10 stimuli at different frequencies; the stimulation intensity was kept at 50% spiking probability for each neuron. Loose-patch recordings were obtained from mature GCs (mat-GC) and 4wpi-GCs to detect spikes. **b.** Raster plots from one mat-GC (left) and one 4wpi-GC (right) at 10 Hz in the control condition (upper panels, black) and after bath application of CBC (lower panels, red). Each color dash denotes a spike. **c.** Average´s sum of action potentials evoked by stimulation trains of 1 Hz, 10 Hz, 20 Hz, and 40 Hz, in mat-GCs (left) and 4wpi-GCs (right) in the control condition (black) or after bath perfusion with CBC (red). CBC increased spiking response of mat-GC but not 4wpi-GC. (mat-GC: two-way ANOVA, variation between control and CBC: ***$p < 0.0001$; variation in frequency: ***$p < 0.001$; interaction: *$p < 0.05$; $N \geq 7$. 4wpi-GC: two-way ANOVA, variation between control and CBC: ns, $p > 0.05$; variation in frequency: ***$p < 0.001$; interaction: ns, $p > 0.05$; $N \geq 9$). **d.** The scheme shows the recording configuration: A stimulating electrode was placed in the mPP to deliver 10 stimuli at 10 Hz while an extracellular recording electrode was placed in the granule cell layer (GCL) to assess population spike (PS, pop spike) responses. Right: Example traces showing the pop spike response to a train of 10 pulses at 10 Hz before (control, upper black) or after bath perfusion with CBC (CBC, bottom red). **e.** Average amplitude of the pop spike response to the 10 Hz train in control (black) and after bath application of CBC (red). CBC increased the pop spike responses in the DG (paired t-test, control vs CBC **$p < 0.01$, $N=6$).

Figure 2. Endogenous release of acetylcholine increases spiking response in the DG.

a. Experimental design. The left image shows a hippocampal slice obtained from adult ChAT-Tom mice with cholinergic terminals expressing tomato (red), but no somas, in the DG. Somas are labeled with DAPI in the upper panel. The right image shows an anterior brain slice obtained from ChAT-Tom mice where the medial septum (MS) and the diagonal band of broca (DB) contain tomato expressing neuronal somas. Scale bar: 500 µm **b.** Experimental scheme, in slices obtained from ChAT-ChR2 mice, we use blue light to activate the cholinergic terminals in the DG. Right, recording configuration: a stimulating electrode was placed in the medial perforant path (mPP) to deliver 10 stimuli at 10 Hz; Extracellular recordings were obtained from the GCL to detect pop-spikes (PS). **c.** Example traces showing the pop spike response to a train of 10 pulses at 10 Hz before (Control, upper black) or after optogenetic stimulation protocol to activate cholinergic terminals (red) (see M&M). **d.** Average amplitude of the pop spike at each pulse (relative to the 1st pulse in control condition) of the 10 Hz train in control (black) and after optogenetic stimutation protocol (red). Optogenetic stimulation increased PS response in the DG (two-way ANOVA, variation between control and optogenetic stimulated: ***$p < 0.0001$; variation between pulses: ***$p< 0.0001$; interaction: **$p < 0.01$). **e.** Average amplitude of the pop spike response to the 10 Hz train in control condition (black) and after light stimulation protocol (red, Opto) with or without the cholinergic antagonists atropine and mecamylamine. Bath perfusion with a combination of atropine and mecamylamine prevented optogenetic induced potentiation of pop spike responses (Paired t-test, Control vs Opto **$p < 0.01$, N = 9; Control vs Opto Atropine *$p < 0.05$, N = 5; Control vs Opto Atropine + Mecamylamine ns $p >0.05$, N = 8).

Figure 3. Cholinergic modulation relies on inhibitory circuits.

a. Recording configuration. Hippocampal slices were obtained from adult ChAT-ChR2 mice. The scheme shows the recording configuration: a stimulating electrode was placed in the medial perforant path (mPP) to deliver 10 stimuli at 10 Hz; Extracellular recordings

were obtained from the GCL to detect pop spikes in presence of the GABA-A antagonist picrotoxin (PTX). **b.** Example traces showing the pop spike response to a train of 10 pulses at 10 Hz (the asterisk denotes the amplitude of the pop spike at each pulse) before (Control, black) or after optogenetic stimulation protocol (Opto, red) to activate cholinergic terminals. **c.** Pop-spike´s average amplitude for each pulse of the 10 Hz train relative to the 1st pulse in the control condition (black) and after optogenetic stimulation (red). **d.** Mean pop spike amplitude in response to the 10 Hz train in control condition (black) and after light stimulation protocol (red, Opto). Light stimulation did not change the pop spike response of GCs in presence of PTX (two-way ANOVA, variation between control and light stimulated: > 0.05; variation between pulses: ***p<0.0001; interaction ns p>0.05, N = 5).

Figure 4. Cholinergic activation decreases evoked inhibitory postsynaptic current (IPSC) onto mat-GCs through nicotinic receptor activation.

a. Experimental scheme. Hippocampal slices were obtained from ChAT-ChR2 mice. Blue light stimulates cholinergic terminals in the DG. Right, recording configuration: A stimulating electrode was placed in the mPP to deliver a train of 10 stimuli at 10 Hz, while whole-cell voltage-clamp recordings were obtained from GCs. Stimulation of the mPP elicits monosynaptic excitation (EPSC) that was recorded at the reversal potential of inhibition (-60mV) and multisynaptic inhibition (IPSC) that was recorded at the reversal potential of excitation (0mV). **b.** Example traces of the IPSCs and EPSCs obtained upon mPP stimulation in control (black) or after blue light stimulation protocol to activate cholinergic terminals (Opto, red). The dashed line shows the time of each stimulus. **c.** Relative EPSC peak at each pulse in control (black) or after light protocol stimulation (Opto, red). Activation of cholinergic axons did not change evoked EPSCs on mat-GCs (Two-way ANOVA, control vs light stimulated: p>0.05; variation in pulse number: ***p<0.001; interaction: p>0.05). **d.** Relative IPSC peak at each pulse in control (black) or after light protocol stimulation (red). Activation of cholinergic axons strongly reduced

evoked IPSCs on mat-GCs (Two-way ANOVA, control vs light stimulated: **p<0.01; variation in pulse number: ****p<0.0001; interaction: ****p>0.0001). **e.** Average excitation/inhibition (E/I) balance elicited by the 10 Hz train in control condition (black) and after light stimulation protocol (red, Opto). Activation of cholinergic axons increases the E/I balance on mat-GCs (paired t-test, control vs light stimulated: ***p<0.001) **f.** Relative IPSC peak at each pulse in control (black) or after light protocol stimulation (Opto, red). Bath application of Mecamylamine prevented cholinergic induced reduction of evoked IPSCs on mat-GCs (Two-way ANOVA, control vs light stimulated: p>0.05; variation in pulse number: ****p<0.0001; interaction: p>0.05)

Figure 5. Acetylcholine specifically reduces feedforward perisomatic evoked IPSC in mat-GCs.

a. Experimental scheme. Hippocampal slices were obtained from ChAT-ChR2 mice. Blue light stimulates cholinergic terminals in the DG. Recording configuration showing the activated circuit. Stimulation of mPP-activated monosynaptic excitation and feedforward inhibition (FFI). Feedback inhibition (FBI) is recruited by the activity of GCs. Application of DCGIV abolished feedback IPSC leaving only the feedforward IPSC (FF-IPSC). **b.** Example trace of evoked FF-IPSC after mPP stimulation with a train of 10 pulses at 10 Hz in control (black), or after blue light stimulation protocol to activate cholinergic terminals (red). **c.** Total inhibitory charge (IPSQ) evoked by the train. Light stimulation significantly reduced the FF-IPSQ (control vs light stimulated: *p<0.05, paired t-test, N=5). **d.** Recording configuration showing the activated circuit. Direct stimulation of the GC activated FBI. The stimulation electrode was placed in the GCL to avoid recruitment of FFI. **e.** Example trace of evoked FB-IPSC after GCL stimulation with a train of 10 pulses at 10 Hz in control (black), or after blue light stimulation protocol (red). **f.** Total IPSQ evoked by the train. Light stimulation did not change the FB-IPSQ (control vs light stimulated: p>0.05, paired t-test, N = 6). **g.** Schematic diagram of the recording configuration. Stimulating electrodes were placed in the GCL and the ML to activate monosynaptic perisomatic or dendritic

inhibition. Experiments were performed in the presence of 6 mM kynurenic acid (Kyn) to block glutamatergic transmission. IPSCs were subsequently measured in whole-cell recordings from individual mat-GCs. Perisomatic IPSCs display a reversal potential of ~0 mV due to the recording conditions under symmetrical Cl^-, while dendritic IPSCs display a positive driving force at that potential. **h.** Example traces of evoked perisomatic (bottom) and dendritic (top) IPSCs from mat-GCs recoded at -70mV in control conditions (black) or after optogenetic stimulation of cholinergic afferents (red). **i.** Optogenetic stimulation produced a decrease in the ratio between perisomatic and dendritic IPSCs relative to control (Paired t-test, control vs light stimulated: **$p < 0.01$, N=5).

Figure 6. Acetylcholine reduces PVI but not SOMI elicited IPSCs in mat-GC.

a. Experimental scheme. PV-Cre mice were stereotaxically injected with the conditional ChR2 adenovirus (AAV-DIO-ChR2) in the DG to induce light evoked action potentials in PVIs from this region. The upper timeline indicates the time of viral injection. 2-6 weeks later, hippocampal slices were obtained from these animals. Blue light trains of 10 pulses at 10 Hz were delivered to the DG while whole-cell recordings were performed on mat-GCs at the reversal potential of excitation (0mV) to record light evoked IPSCs. **b.** Example trace showing light evoked IPSCs in control condition (black) or after bath application of CBC (red). The dash indicates the time of the stimulus. **c.** IPSC peak at each pulse relative to the 1st pulse in the control condition (black) or after bath application of CBC (red). CBC strongly reduced PV-to-GC IPSCs (two-way ANOVA, control vs CBC: **$p < 0.01$; variation in pulse number: ***$p < 0.001$; interaction: **$p < 0.01$, N=9). **d.** Experimental scheme. The experimental design was identical to (**a**) but SOM-Cre animals were used in order to specifically activate this subpopulation of interneurons in the DG. **e.** Example trace showing light evoked IPSCs in control condition (black) or after bath application of CBC (red). The dash indicates the time of the stimulus. **f.** IPSC peak at each pulse relative to the 1st pulse in the control condition (black) or after bath application of CBC (red). CBC did not

change SOM-to-GC IPSCs (two-way ANOVA, control vs CBC: $p > 0.05$; variation in pulse number: ***$p < 0.001$; interaction: $p>0.05$, N=7).

Figure 7. Cholinergic modulation shifts the evoked E/I balance of PVIs vs SOMIs in opposite directions.

a. Recording configuration: Hippocampal slices were obtained from PV-Tom mice. Stimulation of mPP activates monosynaptic excitation and disynaptic inhibition onto PVIs. Whole-cell voltage-clamp recordings were obtained from PVIs in response to stimulation of mPP with trains at 10Hz. **b.** Example trace of evoked postynaptic currents after mPP stimulation with a train of 10 pulses at 10Hz in control (dark blue) or after bath application of CBC (light blue). IPSCs were recorded at the reversal potential of excitation (0mV), and EPSCs were recorded at the reversal potential of inhibition (-70mV). **c.** CBC significantly increased the total evoked IPSQ in PVIs relative to control (Control vs CBC *$p<0.05$, paired t-test, N=4). **d.** E/I balance at each pulse relative to the 1st pulse before (Control, dark blue) or after bath application of CBC (light blue). CBC significantly reduced the E/I balance of PV interneurons (two-way ANOVA, control vs CBC: *$p<0.05$; variation in pulse number: **$p<0.01$; interaction: **$p<0.01$, N= 4). (E) Top, experimental scheme. Hippocampal slices were obtained from SOM-Tom mice. The recording configuration was the same as in (**a**). **f.** Example trace of evoked postynaptic currents after mPP stimulation with a train of 10 pulses at 10Hz in control (purple) or after bath application of CBC (pink). IPSCs were recorded at the reversal potencial of excitation (0mV), and EPSCs were recorded at the reversal potential of inhibition (-70mV). **g.** CBC significantly decreased the total evoked IPSQ in SOMIs relative to control (Control vs CBC *$p<0.05$, paired t-test). **h.** E/I balance at each pulse relative to the 1st pulse in control condition (purple) or after bath application of CBC (pink). CBC significantly increased the E/I balance of SOMIs (two-way ANOVA, control vs CBC: *$p<0.05$; variation in pulse number: **$p<0.01$; interaction: *$p<0.05$ N=6).

Figure 8. High frequency stimulation produces LTP in the DG when paired with optogenetic activation of cholinergic terminals.

a. Experimental scheme. Hippocampal slices were obtained from ChAT-ChR2 mice. A stimulating electrode was placed in the medial perforant path (mPP) to deliver a baseline (0.05 Hz) or a high frequency stimulation protocol (HFS, 4 trains, 500 ms each, 100 Hz within the train, repeated every 20 s) with or without blue light activation of cholinergic terminals. **b.** Temporal evolution of the relative fEPSP slope along the experiment (average from 5 experiments). The black arrow indicates the time at which the HFS protocol was delivered; blue bar indicates the time at which blue light (4 trains, 5000 ms each, 20 Hz within the train repeated every 20s) was delivered. **c.** Average fEPSP slope before (baseline), 10 min after HFS (HFS) and 10 min after pairing light and electrical stimulation (HFS + Light). HFS was insuficient to produce potentiation of the fEPSP unless paired with light activation of cholinergic axon (One-way ANOVA: ***$p<0.001$, Tukey's multiple comparisons: Baseline vs HFS $p>0.05$; Baseline vs HFS + Light *$p<0.05$). **d.** Temporal evolution of the relative fEPSP slope along the experiment (average from 6 slices). Electrical stimulation was kept constant at a frequency of 0,05Hz. Blue bar indicates the time at which blue light (4 trains, 5000 ms each, 20 Hz within the train repeated every 20s) was delivered. **c.** Average fEPSP slope before (baseline), 10 min after pairing optogenetic stimulation. Optogenetic activation of cholinergic terminals was insuficient to produce potentiation of the fEPSP when the mPP was stimulated at low frequency (Paired t-test: Baseline vs Opto $p>0.05$, N=9).

Figure 1

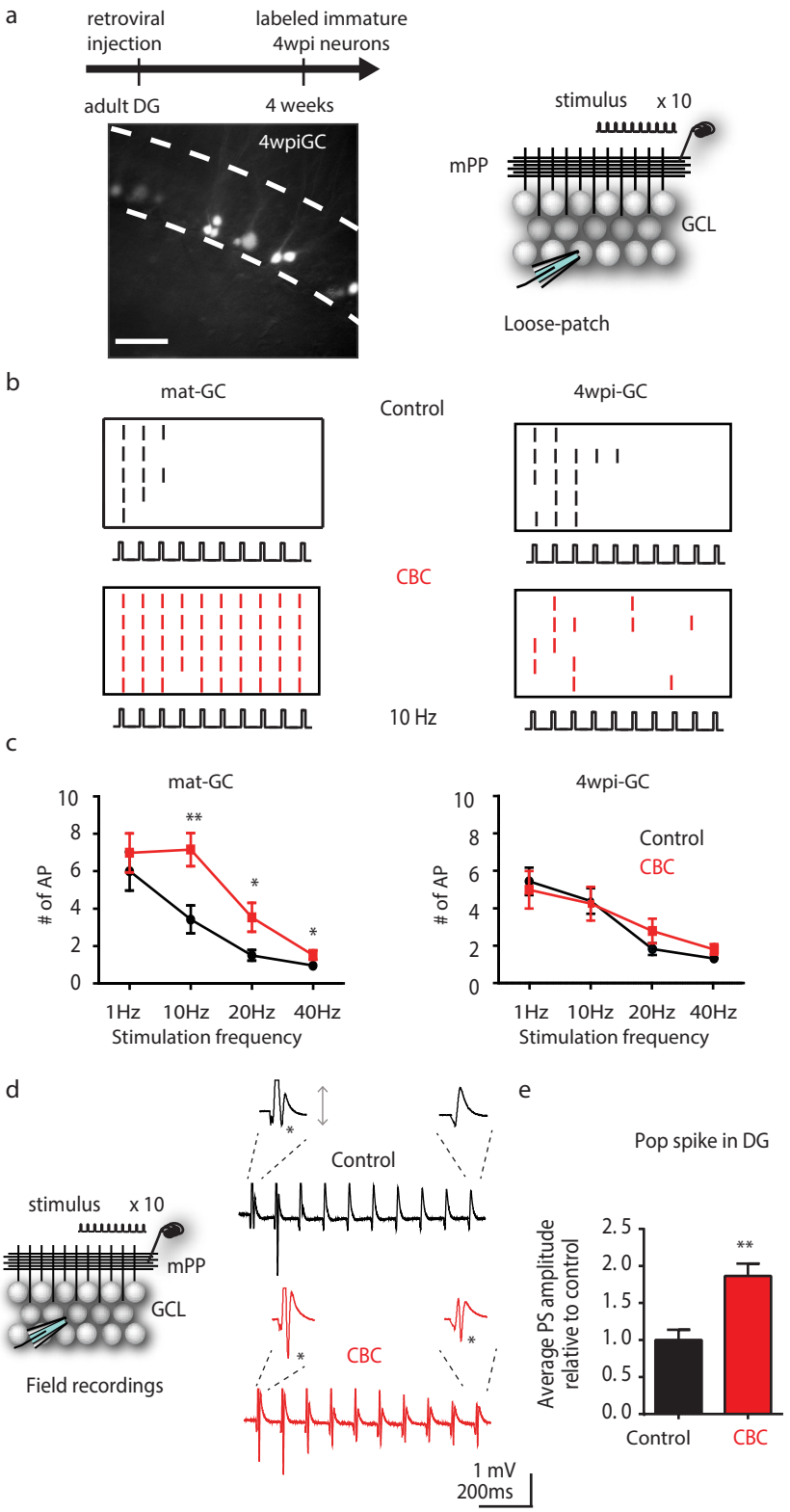
a
retroviral injection
labeled immature 4wpi neurons
adult DG
4 weeks
4wpiGC
stimulus
x 10
mPP
GCL
Loose-patch
b
mat-GC
Control
4wpi-GC
CBC
10 Hz
c
mat-GC
4wpi-GC
# of AP
Control
CBC
1Hz
10Hz
20Hz
40Hz
Stimulation frequency
d
stimulus
x 10
mPP
GCL
Field recordings
Control
CBC
1 mV
200ms
e
Pop spike in DG
Average PS amplitude relative to control
Control
CBC

Figure 2

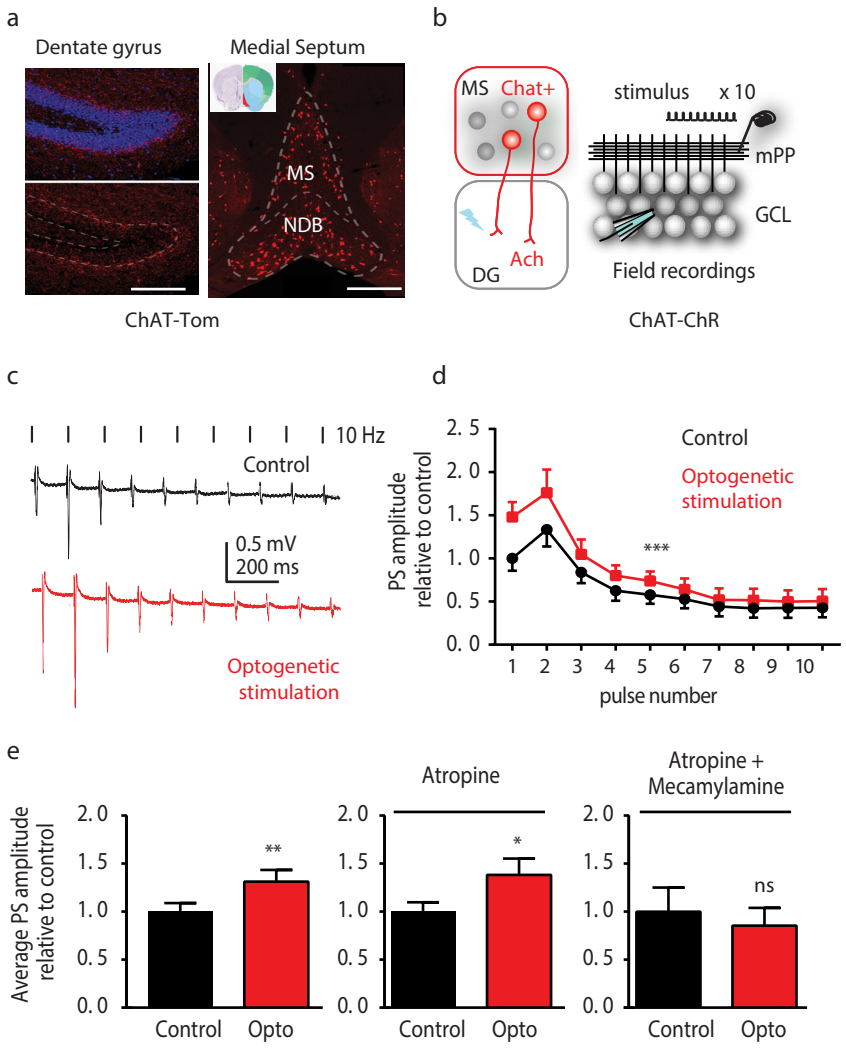
a
Dentate gyrus
Medial Septum
MS
NDB
ChAT-Tom
b
MS
Chat+
Ach
DG
stimulus
x 10
mPP
GCL
Field recordings
ChAT-ChR
c
10 Hz
Control
0.5 mV
200 ms
Optogenetic stimulation
d
Control
Optogenetic stimulation
***
PS amplitude relative to control
pulse number
e
Average PS amplitude relative to control
Control
Opto
**
Atropine
*
Atropine + Mecamylamine
ns

Figure 3

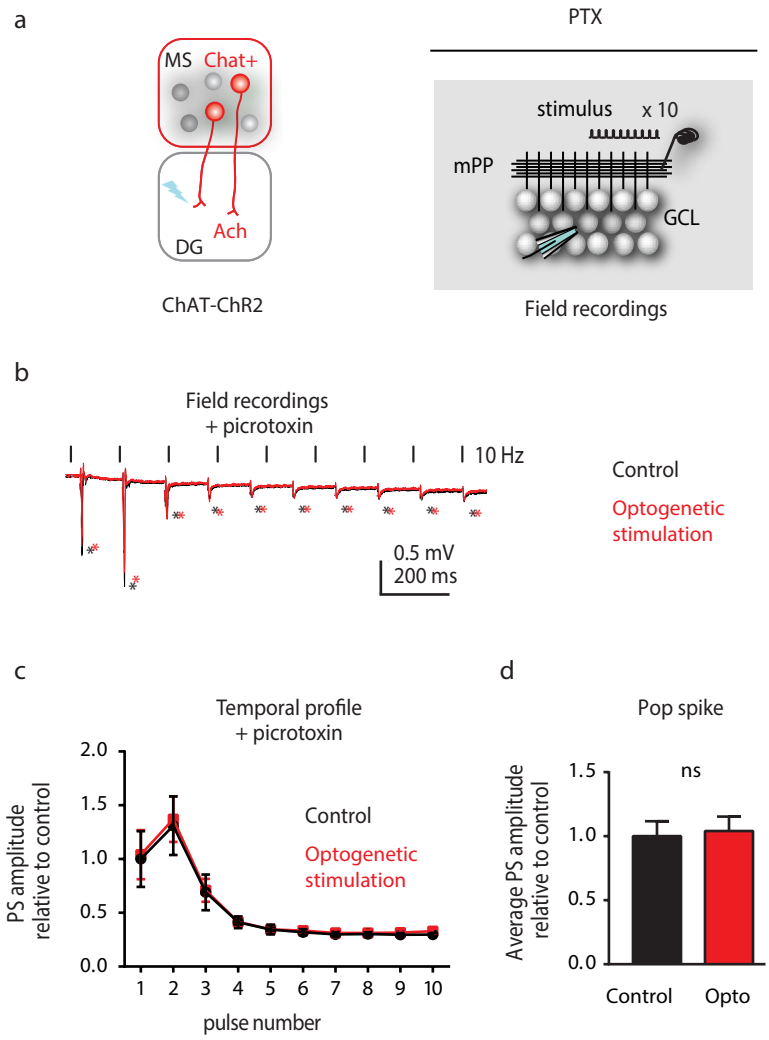
a
MS
Chat+
Ach
DG
ChAT-ChR2
PTX
stimulus
x 10
mPP
GCL
Field recordings
b
Field recordings
+ picrotoxin
10 Hz
0.5 mV
200 ms
Control
Optogenetic
stimulation
c
Temporal profile
+ picrotoxin
PS amplitude
relative to control
2.0
1.5
1.0
0.5
0.0
1 2 3 4 5 6 7 8 9 10
pulse number
Control
Optogenetic
stimulation
d
Pop spike
Average PS amplitude
relative to control
1.5
1.0
0.5
0.0
ns
Control
Opto

Figure 4

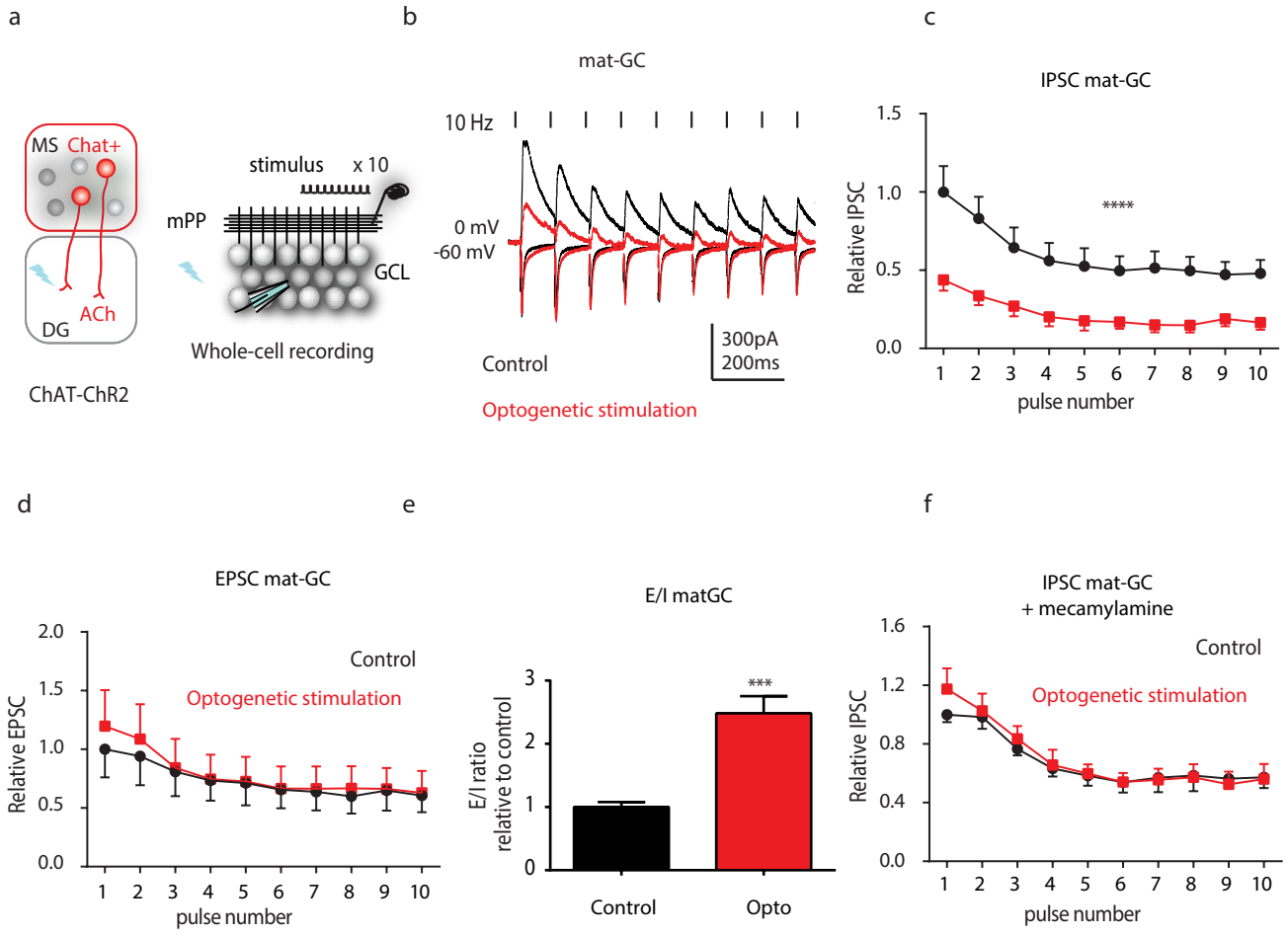
a
MS
Chat+
ACh
DG
ChAT-ChR2
mPP
stimulus
x 10
GCL
Whole-cell recording
b
mat-GC
10 Hz
0 mV
-60 mV
300pA
200ms
Control
Optogenetic stimulation
c
IPSC mat-GC
Relative IPSC
****
pulse number
d
EPSC mat-GC
Relative EPSC
Control
Optogenetic stimulation
pulse number
e
E/I matGC
E/I ratio
relative to control
***
Control
Opto
f
IPSC mat-GC
+ mecamylamine
Relative IPSC
Control
Optogenetic stimulation
pulse number

Figure 5

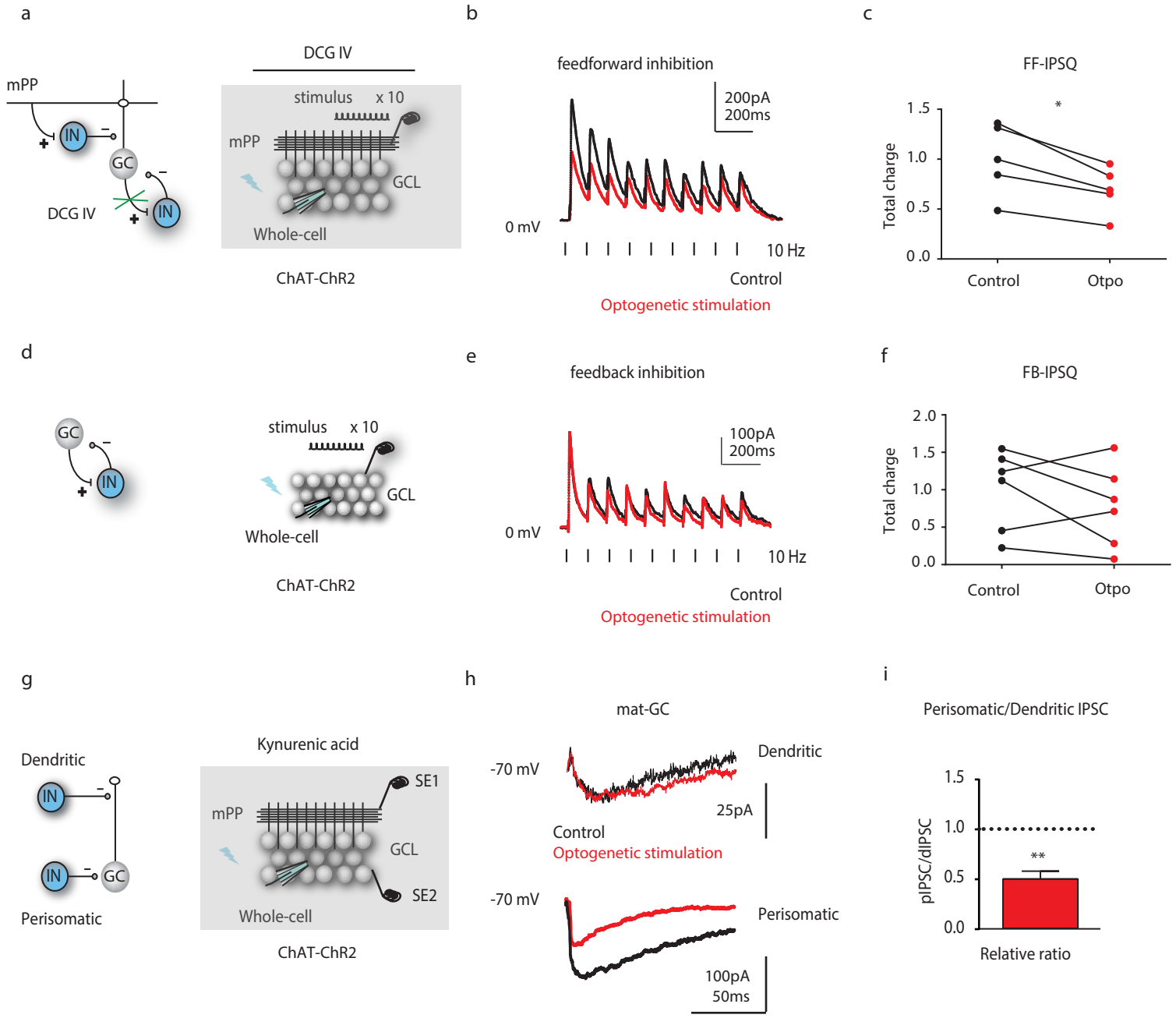
a
mPP
IN
GC
DCG IV
IN
DCG IV
stimulus x 10
mPP
GCL
Whole-cell
ChAT-ChR2
b
feedforward inhibition
200pA
200ms
0 mV
10 Hz
Control
Optogenetic stimulation
c
FF-IPSQ
Total charge
1.5
1.0
0.5
0.0
*
Control
Otpo
d
GC
IN
stimulus x 10
GCL
Whole-cell
ChAT-ChR2
e
feedback inhibition
100pA
200ms
0 mV
10 Hz
Control
Optogenetic stimulation
f
FB-IPSQ
Total charge
2.0
1.5
1.0
0.5
0.0
Control
Otpo
g
Dendritic
IN
IN
GC
Perisomatic
Kynurenic acid
SE1
mPP
GCL
SE2
Whole-cell
ChAT-ChR2
h
mat-GC
-70 mV
Dendritic
25pA
Control
Optogenetic stimulation
-70 mV
Perisomatic
100pA
50ms
i
Perisomatic/Dendritic IPSC
pIPSC/dIPSC
1.5
1.0
0.5
0.0
**
Relative ratio

Figure 6

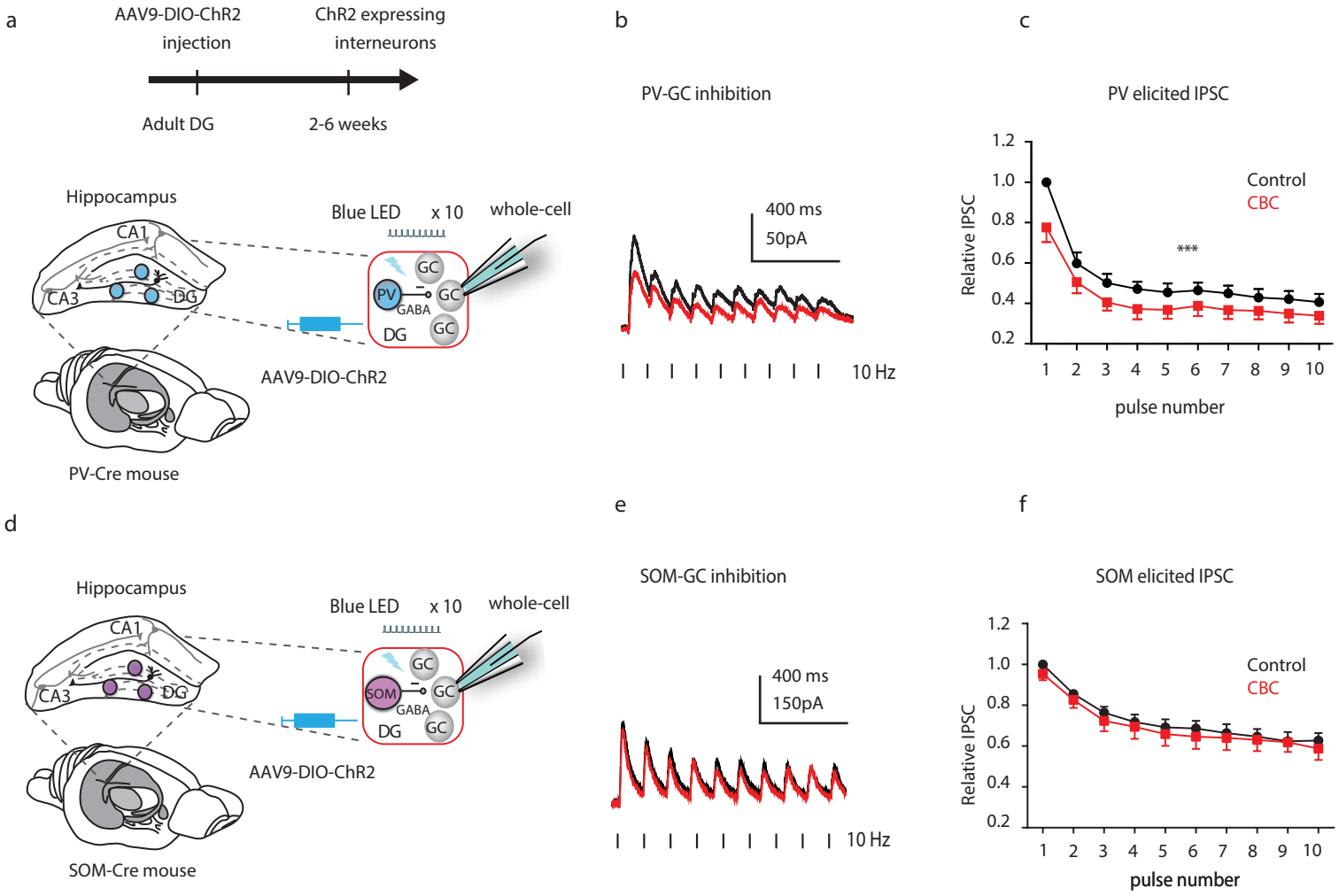
a
AAV9-DIO-ChR2
injection
ChR2 expressing
interneurons
Adult DG
2-6 weeks
Hippocampus
CA1
CA3
DG
Blue LED
x 10
whole-cell
PV
GC
GABA
DG
AAV9-DIO-ChR2
PV-Cre mouse
b
PV-GC inhibition
400 ms
50pA
10 Hz
c
PV elicited IPSC
Control
CBC
***
Relative IPSC
pulse number
d
Hippocampus
CA1
CA3
DG
Blue LED
x 10
whole-cell
SOM
GC
GABA
DG
AAV9-DIO-ChR2
SOM-Cre mouse
e
SOM-GC inhibition
400 ms
150pA
10 Hz
f
SOM elicited IPSC
Control
CBC
Relative IPSC
pulse number

Figure 7

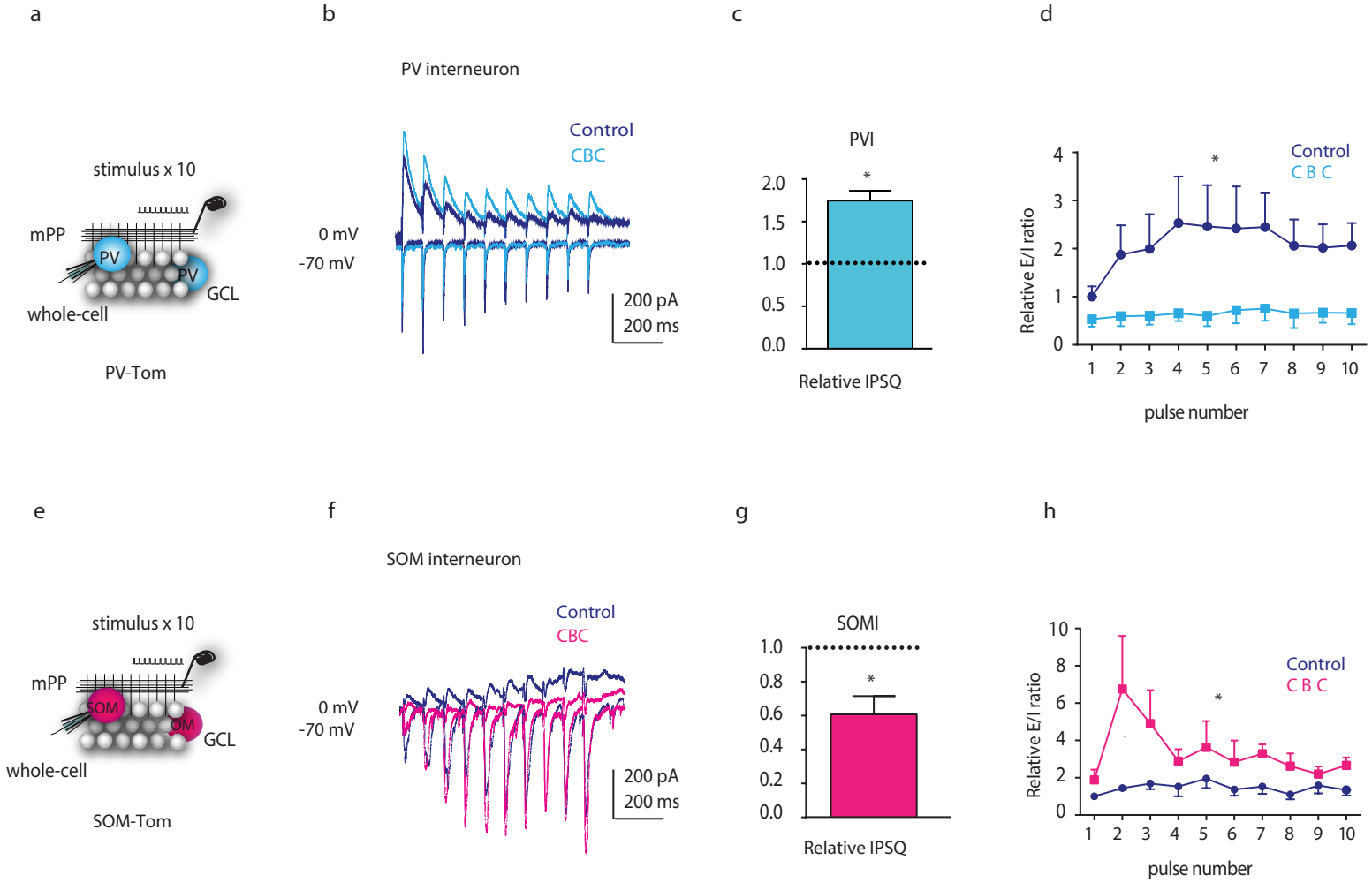
a
stimulus x 10
mPP
PV
PV
GCL
whole-cell
PV-Tom
b
PV interneuron
Control
CBC
0 mV
-70 mV
200 pA
200 ms
c
PVI
2.0
1.5
1.0
0.5
0.0
*
Relative IPSQ
d
Control
C B C
Relative E/I ratio
pulse number
e
stimulus x 10
mPP
SOM
OM
GCL
whole-cell
SOM-Tom
f
SOM interneuron
Control
CBC
0 mV
-70 mV
200 pA
200 ms
g
SOMI
1.0
0.8
0.6
0.4
0.2
0.0
*
Relative IPSQ
h
Control
C B C
Relative E/I ratio
pulse number

Figure 8

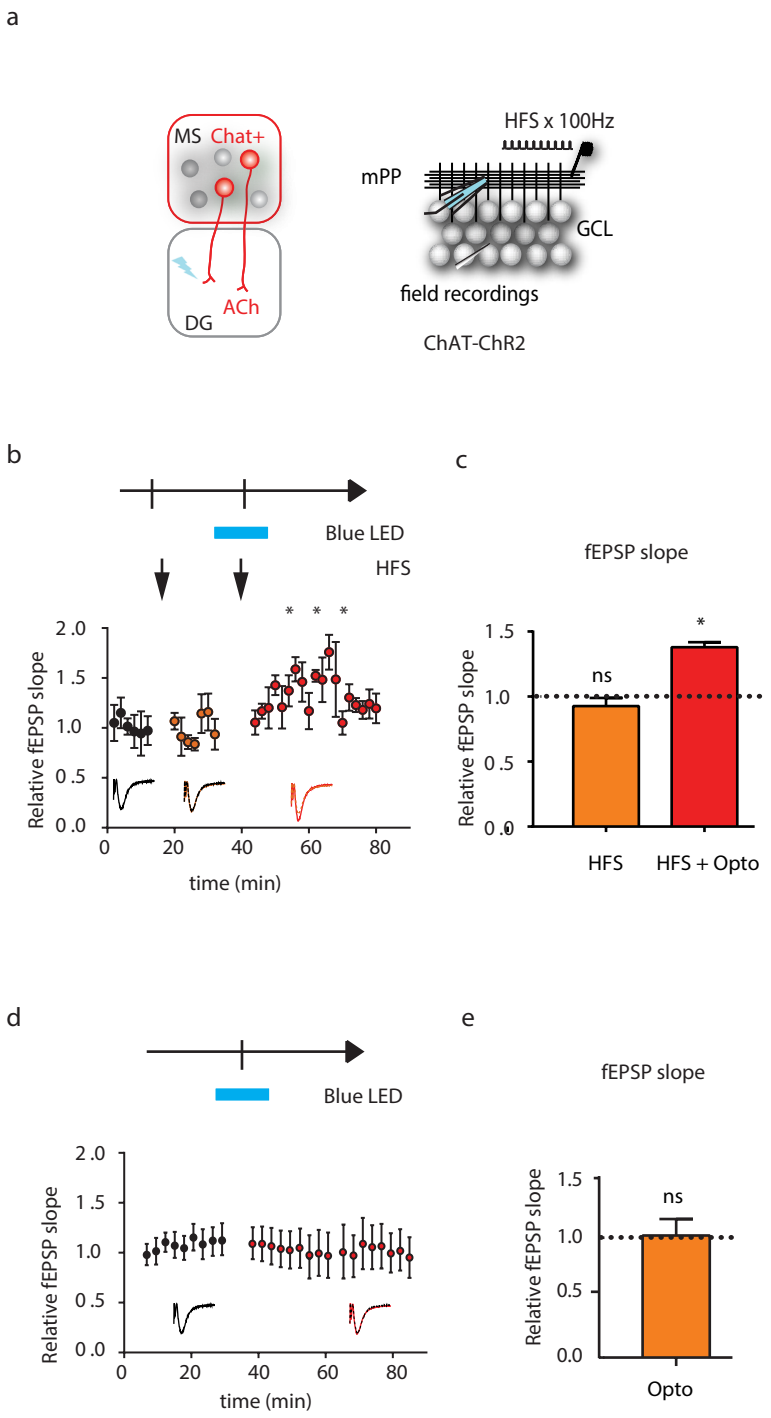
a
MS
Chat+
ACh
DG
HFS x 100Hz
mPP
GCL
field recordings
ChAT-ChR2
b
Blue LED
HFS
Relative fEPSP slope
time (min)
c
fEPSP slope
ns
*
HFS
HFS + Opto
d
Blue LED
Relative fEPSP slope
time (min)
e
fEPSP slope
ns
Opto